Localization versus incommemsurability for finite boson system in one-dimensional disordered lattice

Barnali Chakrabarti[1,2,*] and Arnaldo Gammal[2]

[1]Department of Physics, Presidency University, 86/1 College Street, Kolkata 700073, India.
[2]Instituto de Física, Universidade de São Paulo, CEP 05508-090, São Paulo-SP, Brazil.

(Dated: July 16, 2025)

We explore few-boson systems in a finite one-dimensional quasiperiodic potential covering the full interaction ranging from uncorrelated to strongly correlated particles. We apply numerically exact multiconfigurational time-dependent Hartree for bosons to obtain the few-body emergent states in a finite lattice for both commensurate and incommensurate filling factors. The detailed characterization is done by the measures of one- and two-body correlations, fragmentation, order parameter. For commensurate filling, we trace the conventional fingerprints of disorder induced localization in the weakly interacting limit, however we observe robustness of fragmented and strongly correlated Mott in the disordered lattice. For filling factor smaller than one, we observe existing delocalization fraction of particles interplay with the introduced disorder in a complex way. For strongly interacting limit, the introduced disorder drags the fragmented superfluid of primary lattice to localization exhibiting characteristics of fragmented Mott localization. For filling factor larger than one in the primary lattice, the extra delocalization always resides on commensurate background of Mott-insulator. We observe beyond Bose-Hubbard physics in the fermionization limit when the pairing bosons fragment into two orbitals- Mott dimerization happens. The introduced disorder first relocates the dimers, then strong disorder starts to interfere with the background Mott correlation. The observed findings present a rich landscape of unconventional localization process in the quasiperiodic potentials and pave the way for engineering exotic quantum many-body states with ultracold atoms.

I. INTRODUCTION

The rapid experimental developments in controlling ultracold atoms in optical lattice enables the investigation of the most remarkable paradigmatic phase transition from coherent superfluid (SF) to localized Mott-insulator (MI) phase [1–3]. The MI characterizes several exotic quantum phenomenon, out of special interest like fractional quantum hall effect [4], metal-insulator phase transition in the strongly correlated quantum matter [5], topological phase transition [6]. Many-body localization [7, 8], Bose glass (BG) phases [1, 9–12], fractal Mott lobes [11, 13, 14], Anderson localization [15–19] are also the challenging research areas in disordered lattice. Experimentally, disorder can be introduced by a bichromatic potential or by random potential [10, 20]. A quasiperiodic potential is formed when a primary lattice of high intensity superposed by a secondary weaker one with incommensurate period. The secondary lattice thus effectively introduces disorder in the onsite energies of the lattice, resulting lattice becomes quasiperiodic displaying local inhomogeneities. The phase diagrams of quasiperiodic systemss have been theoretically studied both in one and two dimensions [13, 21–23]. Controlled quasiperiodic potentials are also realized in the experiments with ultracold atoms [24–28].

The one-dimensional quasiperiodic lattice is the most versatile platform to understand localization versus delocalization. For the commensurate filling, interacting bosons in the regular periodic lattice exhibits incompressible Mott insulating phase, whereas for the incommensurate filling an extended superfluid with global correlation is expected. When bosons in the periodic lattice shows a transition from MI to SF phase, in the disordered lattice, the MI to SF transition is intercepted by a compressible but non-coherent phase-Bose Glass phase. In recent studies, the interplay between commensuration and localization has been studied both theoretically and experimentally [14, 29]. It has been illustrated that when the number of particles commensurate with the number of lattice sites, a localized Mott phase in the periodic lattice turns to be delocalized superfluid in the quasiperiodic lattice [14]. It is claimed that the anomalous delocalization is introduced due to interplay between the interaction and commensuration. Whereas Ref. [29] presents the expected features for weakly correlated Mott, but strongly correlated Mott exhibits stringent competition between Mott correlation and correlation due to disorder, which results to melting of Mott localization.

Rapid advancement in experimental techniques have made it possible to study ultracold atomic gases consisting of only tens to hundreds of particles. Sophisticated trapping methods, unprecedented control over experimental techniques like optical pumping [30, 31], geometric constructions [32], evaporative cooling [33], optical tweezers [34] have enabled to control highly correlated small scale systems. In these finite sized systems, quantum fluctuations are enhanced due to reduced particle number. The situation becomes more fascinating in the strongly interacting limit and reduced dimension [35], making it the ideal platform to understand underlying

* barnali.physics@presiuniv.ac.in

microscopic information and emergent quantum phases.

In this paper, we consider a few-boson ensemble in a finite 1D quasiperiodic lattice with various incommensurable setups. The motivation is to understand how the delocalization due to incommensurate fraction of particles in the periodic lattice competes to the localization introduced by disorder in the quasiperiodic lattice. The scenario is different for the filling factor less than or more than one. For filling factor less than one, the delocalization is justified due to poor population. For filling factor more than one, there is extra delocalized particles sitting on the commensurate background of localized particles. The challenging question is how the disorder introduced by the secondary incommensurate lattice will interplay with the existing delocalized fraction of particles in the primary lattice and determine the localization process.

We consider a typical setup of $S = 7$ lattice sites of fixed lattice depth and different incommensurate setups are created by changing the number of bosons. However to unravel the key role played by the incommensurate filling, we also include the study for commensurate setup. We cover the different interaction regimes from the weakly correlated to the fermionization limit when bosons try to escape their spatial overlap. We go beyond the Bose-Hubbard model which assumes unperturbed Wannier orbitals and is restricted to the lowest band. However, one needs to typically include higher band effects to examine the fermionization and strong correlation effects. This is also to mention that this finite sized lattice can be treated as the ideal test bed for the investigation of fundamental building blocks of many-body systems from a bottom-up perspective [36, 37]. Few atoms in the strongly interacting limit are highly correlated and needs an *ab initio* many-body approach. The finite-sized ensemble addressed in the present work will be handled numerically with high precision to capture the correct physics. Thus the observed study can be taken as the 'finite-size precursor' of macroscopic phases in the thermodynamic limit.

We investigate the ground state properties from a bottom-up *ab initio* perspective using multiconfigurational time dependent Hartree for bosons (MCTDHB), which is numerically exact and is an efficient technique for treating the interacting bosons specially in the strong interaction regime when the interatomic correlation plays a significant role [38–40]. We explore the ground states as a function of increasing interaction strength for different filling factor. We analyze the one- and two-body densities, fragmentation to understand the complex interplay between disorder and existing delocalization in the primary lattice.

We consider the following set ups in the periodic lattice and further investigate their response in the presence of secondary lattice. a) commensurate filling, filling factor $\nu = \frac{N}{S} = 1$, $N = 7$ bosons are in $S = 7$ lattice sites. For weak interaction, we retrieve the usual localization process, although find robustness of strongly correlated Mott in the fermionization limit. b) Incommensurate filling factor $\nu < 1$, $N = 5$ bosons are in $S = 7$ lattice sites. For weak interaction, although very strong disorder introduces central localization, some unseen features is observed in the strongly interacting limit. We observe that disorder drags the fragmented superfluid of the primary lattice to the fully fragmented localized phase. c) Incommensurate filling $\nu > 1$ exhibits more intriguing competition between delocalization due to repulsion, on-site interaction and localization due to disorder. There is always N mod S particles at the background of Mott localization with unit filling. The extra particle/particles lie in the Mott background, in the fermionization limit they form one or more dimers. The introduced disorder displaces the dimers' position when the background Mott correlation does not change significantly.

The paper is organized as follows. In Sec II, we present the system we study. In Sec III, we give a brief review of the method we employ to investigate the system numerically exactly. In this section we also define the observables used to understand different features. In Sec. IV, we present results for commensurate filling. In Sec. V, we present results for incommensurate filling distributed over two subsections. We conclude our findings in Sec. VI.

II. SYSTEM AND PROTOCOL

We investigate the ground state of N interacting bosons of mass m in a one-dimensional quasiperiodic lattice. The Hamiltonian can be written as

$$\hat{H}(x_1, x_2, \dots x_N) = \sum_{i=1}^{N} \hat{h}(x_i) + \sum_{i<j=1}^{N} \hat{W}(x_i - x_j), \quad (1)$$

where x_i corresponds to the coordinate of each particle. The one-body part of the Hamiltonian is $\hat{h}(x) = \hat{T}(x) + \hat{V}_{OL}(x)$, where $\hat{T}(x) = -\frac{\hbar^2}{2m}\frac{\partial^2}{\partial x^2}$ is the kinetic energy operator and $\hat{V}_{OL}(x) = V_p \sin^2(k_p x) + V_d \sin^2(k_d x)$ is an external potential characterized by two interfering standing waves that generate a quasiperiodic lattice. The Hamiltonian in Eq. (1) can be written in dimensionless units obtained by dividing the dimensionful Hamiltonian by $\frac{\hbar^2}{m\bar{L}^2}$, with $\bar{L}$ an arbitrary length scale. For the sake of our calculations, we will set $\bar{L}$ to be the period of the primary optical lattice.

The quasiperiodic potential consists of a primary lattice of depth V_p and wave vector k_p perturbed by a secondary weaker lattice of depth V_d, wave vector k_d. When the ratio of the two wave vectors k_p/k_d is chosen to be incommensurate, the external potential generates a regular but non-repeating structure that implements correlated disorder on top of the periodic primary lattice. In the experiment by Roati et al. [24, 41], k_p and k_d were chosen such that the inverse of the golden ratio $\Phi = \frac{\sqrt{5}-1}{2}$ becomes the target incommensuration parameter. In the actual experiment, the choice of wavelengths are $\lambda_p = \frac{2\pi}{k_p} = 1032$ nm and $\lambda_d = \frac{2\pi}{k_d} = 862$ nm, leading to an incommensurate ratio $\frac{k_d}{k_p} \simeq 1.1972157773....$ However, in the computation, the incommensurate frequency ratio used to generate the quasiperiodic potential will necessarily be approximated by a rational number due to finite numerical precision. We have verified that this approximation preserves the quasiperiodic features within the limits of the numerical grid used in the numerical simulation. Unless otherwise stated, we will keep the wave vectors fixed at $k_p = 1.0$ and $k_d = 1.19721$. For the entire calculation we fix $V_p = 10E_r$ and probe various values of the potential depths $V_d \in [0E_r, 3E_r]$, where $E_r = \frac{\hbar^2 k_p^2}{2m}$ is the recoil energy of the primary lattice.

In the entire computation, we restrict the system geometry to accommodate $S = 7$ sites in the primary optical lattice which is defined as the spatial extent between two maxima in the sinusoidal function and adding hard-wall boundary conditions at each end. The typical case with seven wells, will well capture all essential features of competition between the attempted localization due to disorder and existing delocalization due to incommensuration. To probe the physics in commensurate filling we choose $N = 7$ particles, whereas for incommensurate filling < 1, $N = 5$ and for > 1, $N = 8$ and $N = 9$ are used.

The two-body interactions $\hat{W}(x_i - x_j)$ appearing in Eq. (1) are modeled as a contact interaction $\hat{W}(x_i - x_j) = \lambda \sum_{i<j} \delta(x_i - x_j)$. λ controls the strength of interaction and it is positive (repulsive interaction) in our entire calculation. To probe the pathway from superfluid to fragmented SF to Mott, fully fragmented Mott and fermionization limit, we probe the interaction strength in the range $\lambda \in [0E_r, 10E_r]$

We will solve the Hamiltonian above numerically exactly to extract the ground state properties of the system and measures the key observables such as, real-space density, and correlations to reveal the fate of the many-body state subject to quasiperiodicity.

III. METHOD

To study the ground-state properties of interacting bosons with correlated quasiperiodic disorder for various filling factor, we employ the MultiConfigurational Time-Dependent Hartree method for indistinguishable particles (MCTDH) [42–47] as implemented in MCTDH-X package [48, 49].

In the MCTDH method, the many-body Schrödinger equation is represented by the many-body wave function as an adaptive, time-dependent superposition of permanents, which are built by distributing N particles into M single-particle wave functions known as orbitals. Both the coefficients and the basis functions in the superposition are optimized over time, enabling the calculation of ground-state properties through imaginary relaxation or the simulation of full-time dynamics using real-time propagation. In this work, we focus exclusively on imaginary time propagation to relax the system to its ground state. We employ the MCTDHB, which is the most advanced algorithmic implementation of the MCTDH approach for the bosons. Further details on this method are contained in Appendix A.

Utilizing several orbitals in the many-body ansatz allows us to capture the beyond mean-field scenario when the many-body state is fragmented- when several orbitals have significant occupation. MCTDHB is exact by construction and the convergence of the method is guaranteed in the limit $M \to \infty$. However in practice, a much smaller set of orbitals is needed to obtain *numerically exact* results. A larger number of orbitals are generally required for strongly interacting bosons to capture many-body correlation effects. We repeat the computation by increasing the number of orbitals and optimized when the results do not change by including more orbitals in the MCTDHB expansion and the occupation in the last orbital becomes insignificant. In the present manuscript we utilize $M = 12$ orbitals.

To study the ground state of the system, we compute various observables from the many-body state $|\Psi\rangle$, the spatial distribution of the bosons is understood calculating the one-body density as

$$\rho(x) = \langle \Psi | \hat{\Psi}^\dagger(x) \hat{\Psi}(x) | \Psi \rangle. \tag{2}$$

To measure the degree of coherence in the many-body wavefunction, we calculate the reduced one-body and two-body density matrices defined as

$$\rho^{(1)}(x, x') = \langle \Psi | \, \hat{\Psi}^\dagger(x) \hat{\Psi}(x') \, | \Psi \rangle \tag{3}$$

$$\rho^{(2)}(x, x') = \langle \Psi | \, \hat{\Psi}^\dagger(x) \hat{\Psi}^\dagger(x') \hat{\Psi}(x') \hat{\Psi}(x) \, | \Psi \rangle \, . \tag{4}$$

Information about the orbital occupations in the ground state is extracted from the reduced one-body density matrix. This is described in terms of the natural orbitals $\phi_i^{(\mathrm{NO})}$ and their occupations ρ_i, which correspond to the eigenfunctions and eigenvalues of $\rho^{(1)}(x, x')$, respectively, as given by

$$\rho^{(1)}(x, x') = \sum_i \rho_i \phi_i^{(\mathrm{NO}),*}(x') \phi_i^{(\mathrm{NO})}(x). \tag{5}$$

We further utilize the eigenvalues of the reduced one-body density matrix to construct an order parameter [50]

$$\Delta = \sum_i \left(\frac{\rho_i}{N} \right)^2 \tag{6}$$

Δ quantifies the loss of coherence and thus maps out the transition from superfluid ($\Delta \to 1$) to fragmented Mott state ($\Delta \to \frac{1}{S}$).

The one-body momentum distribution is constructed from

$$n(k) = \int dx \int dx' \, e^{-ik(x - x')} \rho^{(1)}(x, x') \tag{7}$$

IV. LOCALIZATION AND CORRELATION IN DISORDERED LATTICE FOR COMMENSURATE FILLING

In this section, we present ground state properties in the periodic and quasiperiodic lattice for the commensurate filling of $N = 7$ bosons in $S = 7$ lattice sites for various interaction strength, ranging from delocalized superfluid in the noninteracting limit to fragmented Mott insulating phase in the fermionization limit. The one-body density is presented in Fig. 1(a). In a periodic lattice, the competition between the kinetic, trap and interaction energy determines the ground state configuration. For the non-interacting case, the kinetic and potential energy competes, and the density is maximal in the central well representing a superfluid phase. However as the interaction strength increases, the bosons redistribute in outer sites due to repulsive interaction. For $\lambda = 0.5E_r$, bosons localize equally in all sites signifying an insulating phase. This Mott-insulator phase is characterized by the localization of atoms in the lattice with a vanishing overlap of the densities in distinct wells. Once localization occurs, the increase in the interaction ($\lambda = 5E_r$) no longer affect the density distribution.

The superfluid-to-Mott-insulator transition is further characterized by fragmentation. In Fig. 1(b), we plot the corresponding occupation of the first $M = 10$ orbitals as a function of the interaction strength as the other two orbitals have insignificant contribution. We use the criterion of Penrose and Onsager [51] to identify whether the many-body state is condensed or fragmented. The system is a condensate if the reduced one-body density matrix has a single macroscopic eigenvalue. For noninteracting case or very very weak interaction, when the first natural orbital is macroscopically occupied and the population of the remaining orbitals is insignificant, the system can be well approximated by the many-body wave function with a single-orbital mean-field state $|N, 0.....\rangle$. With increase in λ, the occupation of the first natural orbital gradually decreases while the occupations of other orbitals gradually increase. For $\lambda = 0.5E_r$, when the one-body density exhibits equal population in all sites, the many-body state is a fragmented Mott state characterized by significant occupations in several orbitals. Whereas a fully fragmented Mott is achieved when the number of contributing orbitals becomes equal to the number of lattice sites and each orbital contributes equally, $\frac{1}{S}$ of total population. In the present set up of commensurate lattice, with further increase in λ, the Mott insulating phase gradually drives to fully fragmented Mott phase- the many-body wave function is a seven-fold fragmented state $|1, 1, 1, 1, 1, 1, 1\rangle$, each orbital contributes $\simeq 14.28\%$. Fig. 1(b) demonstrates the transition from SF to MI to fragmented MI phase.

To illustrate how the correlated disorder modifies the density signature in the primary lattice, we further study the one-body reduced density matrix $\rho^{(1)}(x, x')$ for several values of V_d. We choose three specific cases of interaction strength.; $\lambda = 0.0$ (superfluid), $\lambda = 0.5$ (Mott-insulating), $\lambda = 5.0$ (fragmented Mott) [Figs. 2(a)-(i)]. In the periodic lattice, it is not possible to distinguish the Mott insulating phase from the fragmented Mott phase from the one-body density (Fig. 1(a)). However, in the quasiperiodic lattice, the response of Mott insulating phase and fully fragmented Mott phase will be different, the later becomes more correlated and remains robust

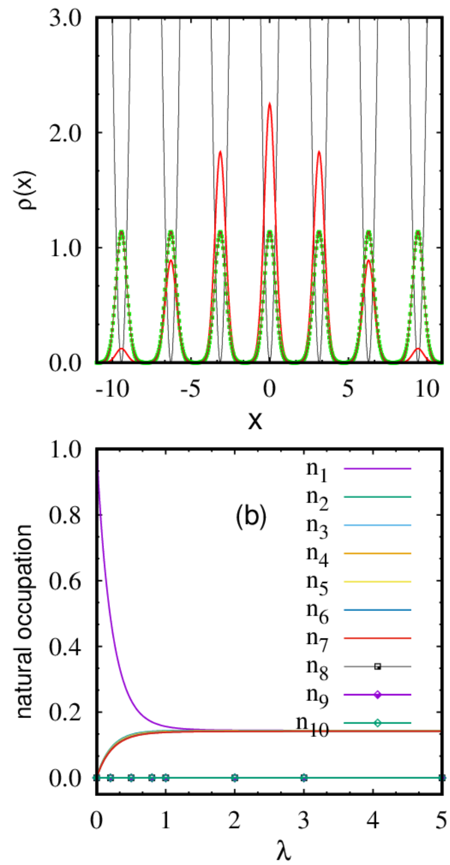

FIG. 1. (a)The one-body density $\rho(x)$ in the primary lattice with seven wells and seven particles for different values of interaction strength. Solid red line, lines with green solid square and brown down triangle correspond to $\lambda = 0E_r, 0.5E_r, 5E_r$ respectively. The gray line represents the primary lattice. For $\lambda = 0E_r$, the density is maximal at the central well- superfluid phase. For $\lambda = 0.5E_r$, the bosons are equally distributed in seven wells- Mott-insulator phase. For higher interaction strength, $\lambda = 5E_r$, one-body density overlaps with the density for $\lambda = 0.5E_r$- Mott localization is maintained. (b) Populations of the first ten natural orbitals as a function of interaction strength. As λ increases, the occupation of the first orbital gradually decreases while other orbitals begin to contribute. Eventually the many-body state becomes seven-fold fragmented ($n_1 \simeq n_2 \simeq n_3 \simeq n_4 \simeq n_5 \simeq n_6 \simeq n_7 \simeq 1/7$ at $\lambda \simeq 2$, the remaining three orbitals have insignificant contributions.

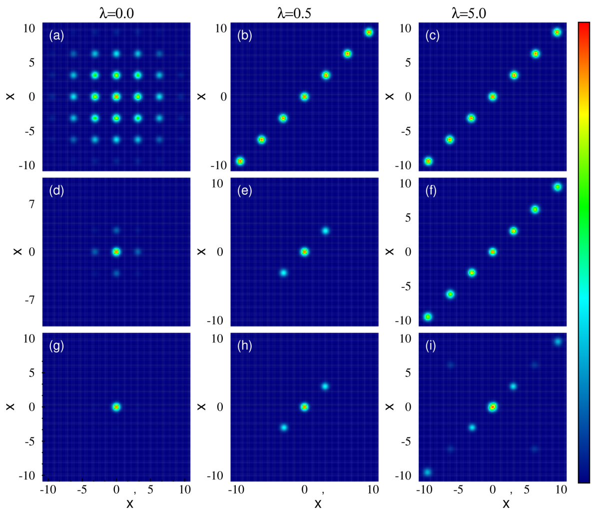

FIG. 2. The reduced one-body density $\rho^{(1)}(x,x')$ for commensurate filling. The panels show a comparison between periodic [$V_d = 0E_r$, panels (a)-(c)] and various choices of quasiperiodicity [panels (d)-(i)]. For $\lambda = 0E_r$, (d): $V_d = 0.01E_r$ and (g): $V_d = 0.05E_r$. For $\lambda = 0.5E_r$, (e): $V_d = 1E_r$ and (h): $V_d = 3E_r$. For $\lambda = 5E_r$, (f): $V_d = 2E_r$ and (i): $V_d = 3E_r$.

even for strong disorder.

For noninteracting case ($\lambda = 0E_r$) and in the periodic lattice ($V_d = 0E_r$), the system is a delocalized superfluid, manifested by the short and long-range correlations and the non-vanishing off-diagonal behavior of $\rho^{(1)}(x,x')$ ((Fig. 2(a)). For such a truly finite lattice system rigorous definition of off-diagonal long-range order is inappropriate, however off-diagonal of $\rho^{(1)}(x,x')$ measures correlation across the lattice. We also observe the off-diagonal correlation is gradually depleted with increasing distance from the central lattice sites. On switching on small disorder ($V_d = 0.01E_r$) immediately destroys the off-diagonal correlation (Fig. 2(d)) and $V_d = 0.05E_r$ leads to localization in the central lattice (Fig. 2(g)) as expected.

When λ increases, the off-diagonal correlation is already depleted in the periodic lattice (Fig. 2(b)). Weak repulsion ($\lambda = 0.5E_r$) pulls the particles away from the middle wells, Mott localization happens. Seven particles are now uniformly distributed in seven lattice sites and only the intra-well correlation is maintained whereas inter-well correlation is completely lost. The diagonal of $\rho^{(1)}(x,x')$ shows seven completely separated coherent regions where $\rho^{(1)} \simeq 1$ and at the off-diagonal $\rho^{(1)} \simeq 0$ (Fig. 2(b)). The Mott localization is maintained even for weak disorder. For sufficiently strong disorder ($V_d = 1E_r$) the Mott localization is gradually destroyed which further leads to localization into middle and two side wells (Fig. 2(e)). However, even very strong disorder ($V_d = 3E_r$), fails to bring central localization (Fig. 2(h)).

The situation is more interesting in the strongly interacting limit $\lambda = 5E_r$, when the Mott insulating phase in the primary lattice is fully fragmented and strongly correlated. Although it is impossible to distinguish the Mott correlation for weak interaction (Fig. 2(b)) and strong interaction (Fig. 2(c)), as in both cases the Mott localization is only manifested by seven bright lobes along the diagonal. However their response in quasiperiodic lattice is different. The less correlated Mott is dragged to localization in the quasiperiodic lattice, whereas strongly correlated Mott remains robust even when the disorder is quite high $V_d = 2E_r$ (Fig. 2(f)). For much stronger disorder, $V_d = 3E_r$ the Mott correlation in the outer lattice sites is slightly depleted but localization in the middle wells does not happen (Fig. 2(i)).

V. LOCALIZATION AND CORRELATION IN DISORDERED LATTICE FOR INCOMMENSURATE FILLING

In this section we like to investigate the consequences of disorder for different incommensurate filling factors both smaller and greater than one. The competition between localization due to stronger interaction and localization due to disorder becomes more fascinating for incommensurate filling due to additional existing delocalization from superfluid fraction. For filling factor less than one, due to less population of particles, on-site interaction does not play the dominating role. In the noninteracting case, disorder introduces the central localization as expected. However in the limit of very strong interaction, particles are already driven away from the central lattice, the introduced disorder by the secondary lattice tries to localize them in the middle lattice sites. We observe that the localized state exhibits the signature of fully fragmented many-body state mimicking the Mott localization. Filling factor more than one, combines the effects of localization due to stronger interaction, on-site interaction and introduced disorder. Extra population of particles manifests on-site effect leading to beyond Bose-Hubbard physics. In the fermionization limit, the lattice site with double occupation forms dimer and the pair fragments into two orbitals in the same well. The additional disorder now competes the situation in a very complex way. In both cases of incommensurate filling we present the key measures - one and two-body correlation functions.

A. Filling factor $\nu < 1$

In this section, we consider the case of incommensurate filling with $\nu < 1$, five bosons in seven wells. Fig. 3 summarizes our main observation, how the particles localize in the lattice in the presence of disorder. Fig. 3(a) represents the ground-state density in the primary lattice for various interaction strength $\lambda = 0E_r, 0.5E_r, 5E_r$. For the noninteracting ground state, the density is larger in the middle sites and decreases as we go to the outer

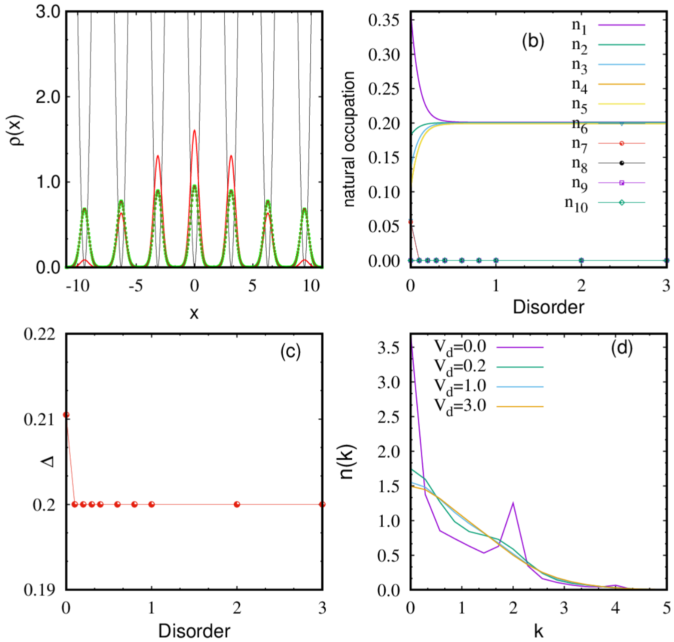

FIG. 3. (a) One-body density $\rho(x)$ in the primary lattice with five bosons in seven lattice sites and for different interaction strength. Solid red line, lines with green solid square and brown down triangle correspond to $\lambda = 0E_r, 0.5E_r, 5E_r$ respectively. The gray line represents the primary lattice. (b) Natural occupations in the lowest $M = 10$ orbitals for $\lambda = 5E_r$ as a function of disorder. (c) Order parameter for $\lambda = 5E_r$ as a function of disorder. (d) Momentum distribution for $\lambda = 5E_r$ and for various disorder parameter V_d.

site. Now the key concern how the particles will distribute themselves in outer sites with increase in interaction strength. In the weakly interacting limit, $\lambda = 0.5E_r$, there is a transfer of particles from the middle wells to the outer wells due to interatomic repulsion. However as the number of particles is smaller than the number of lattice sites ($N < S$), one-particle density does not tend to an equal site occupation even in the strongly interacting limit $\lambda = 5E_r$.

To understand the response of the system in the presence of secondary lattice, we utilize several key measures as a function of disorder strength : fragmentation, order parameter, one-body momentum distribution, one-body and two-body correlation function. For the noninteracting case, disorder simply introduces localization in the central lattice as expected and is not shown here. The rest of the analysis in this section is focused for strongly interacting limit, $\lambda = 5E_r$, when some intriguing features are expected. In Fig. 3(b), we present the fragmentation analysis of natural orbitals. The relative population n_i in different natural orbitals defines the degree of fragmentation. For a nonfragmented condensate the highest occupation in the lowest natural orbital $\simeq 1$. Fragmentation happens when more than one natural orbital exhibits significant population. The computation is done with $M = 12$ orbitals and in Fig. 3(b), we present normalized population in lowest $M = 10$ natural orbitals (as the population in the other two orbitals is $< 10^{-6}$) as a function of the disorder strength V_d. When a single eigenvalue is macroscopic, the state is a superfluid. However, for $V_d = 0E_r$, the ground state is already fragmented, as several orbitals contribute, it is a fragmented superfluid due to strong interaction. With increase in V_d, the occupation of the first natural orbital gradually decreases while the occupations of the second, third, fourth and fifth orbitals gradually increase. For $V_d = 0.5E_r$, the first five natural occupations equally saturate at 20%, all other remaining orbitals had occupations smaller than 10^{-6}, thus leading to five-fold fragmentation. This five-fold fragmentation indicates the transition to the five-fold fragmented localized phase which persists even for very strong disorder. Thus introduced disorder drags the fragmented superfluid to a insulating phase localized in five middle sites. Generally, a fully fragmented Mott-insulating phase is characterized when there are as many significant eigenvalues of the reduced density matrix as there are lattice sites. Thus strongly interacting fragmented superfluid of $N = 5$ bosons in the primary lattice settles to fully-fragmented localized insulating phase in the $S = 5$ middle sites in the presence of secondary lattice, thus characterizing similar features of Mott localization. The transition can be more clearly inferred from the one- and two-body correlation functions as discussed later.

In Fig. 3(c), we show the order parameter $\triangle$, as a function of detuning lattice depth V_d. When superfluid exhibits a single orbital occupation, typically $\triangle \simeq 1$. As Mott insulating phase exhibits equally distributed density over multiple orbitals and sites $\triangle \simeq \frac{1}{S}$. Fig. 3(c) exhibits that in the primary lattice, the initial state is already fragmented due to strong interaction. With increase in V_d, the insulating phase emerges when $\triangle$ reaches to $\frac{1}{S} = 0.2$, i.e., the five-fold fragmentation happens.

In Fig. 3(d), we observe that the momentum distribution exposes a rich pattern with Bragg peaks for $V_d = 0E_r$. The central peak is also high, signifying the presence of off-diagonal long-range order. With increase in V_d, the Bragg peak is gradually smeared, the central peak is substantially lowered which is a typical signature of loss of long-range correlation due to localization.

In Fig. 4, we present both the one- and two body correlations for the incommensurate setup with five bosons in seven wells in the strongly interacting limit with $\lambda = 5E_r$. The left column corresponds to one-body and the right column corresponds to two-body correlation for various de-tuning lattice depth V_d. The main difference between the commensurate and incommensurate filling, is the off diagonal part of reduced one-body density matrix can not vanish completely due to the presence of delocalized superfluid. In the clean lattice, the one-body correlation is mostly concentrated along the diagonal, however not equally distributed in all sites. There is a quite well local-

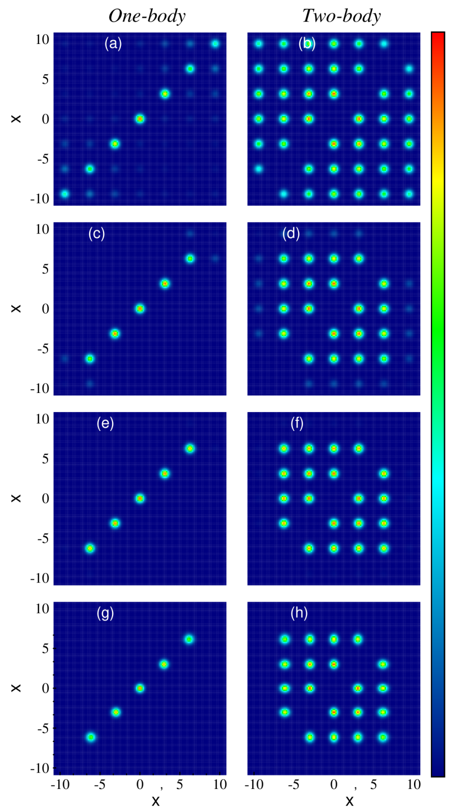

FIG. 4. The reduced one-body density $\rho^{(1)}(x, x')$ (left column) and two-body density $\rho^{(2)}(x, x')$ (right column) for five bosons in seven wells with interaction strength $\lambda = 5E_r$. The panels show comparison between periodic case $[V_d = 0E_r, (a) - (b)]$ and the quasiperiodic cases [panels (c)-(h)]. $V_d = 0.1E_r$ [(c)-(d)], $V_d = 0.5E_r$ [(e)-(f)], $V_d = 3E_r$ [(g)-(h)]

ization around the middle lattice sites, with vanishing off-diagonal correlation. Whereas in the distant lattice sites, localization is poor which is also confirmed by the presence of off-diagonal correlation (Fig. 4(a)). The two-body correlation in the clean lattice shows an almost depleted diagonal implying $\rho^{(2)}(x, x) \to 0$, probability of finding two bosons in the same lattice is zero. The square-lattice like pattern with a missing diagonal is the hallmark of insulating phase. However in Fig. 4(b), for $V_d = 0E_r$, the two-body off-diagonal coherence is not uniform signifying the nonuniform localization of the particles and presence of delocalized superfluid fraction. On switching on the disorder potential, $V_d = 0.1E_r$, it immediately dominates and eliminates the existing delocalization of the primary lattice (Fig. 4(c)-(d)). For $V_d = 0.5E_r$, five bosons localize in the five central lattice sites. Five fully coherent bright spots along the diagonal signifies localization happens in the five middle sites while two outer lattice sites remain empty (Fig. 4(e)). The two-body correlation function with completely extinguished diagonal and uniform off-diagonal correlation also settles around the five middle lattice sites (Fig. 4(f)). The feature remains same even for very strong disorder $V_d = 3E_r$ (Fig. 4(g)-(h)).

B. Filling factor $\nu > 1$

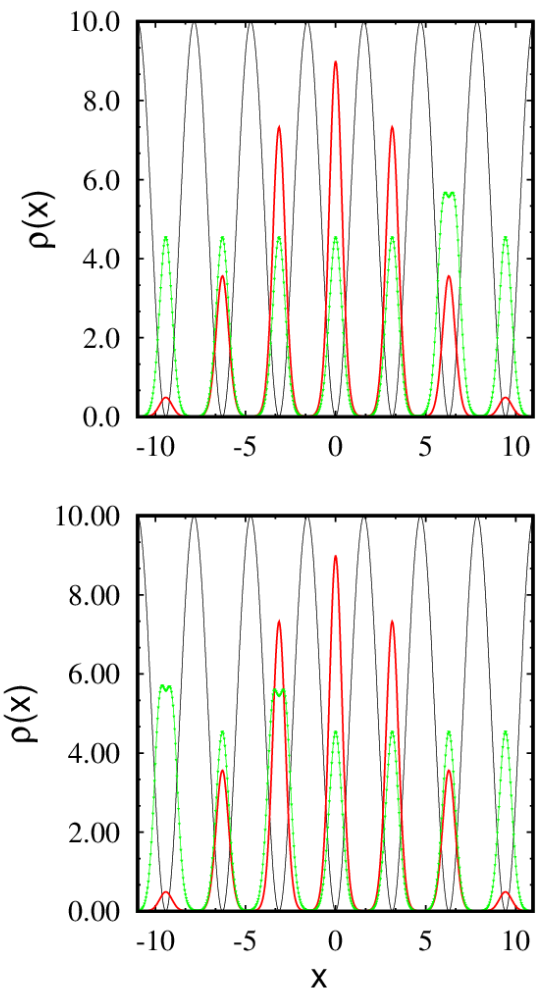

FIG. 5. (Top panel) One-body density $\rho(x)$ in the primary lattice with eight bosons in seven lattice sites and for different interaction strength. Solid red line corresponds to noninteracting case ($\lambda = 0E_r$). The green line corresponds to fermionization limit ($\lambda = 10E_r$). (Bottom panel) One-body density $\rho(x)$ in the primary lattice with nine bosons in seven lattice sites and for different interaction strength. Solid red line corresponds to noninteracting case ($\lambda = 0E_r$). The green line corresponds to fermionization limit ($\lambda = 10E_r$). The gray line represents the primary lattice. Characteristic dips signify the formation of dimers.

For a filling factor more than one, when N mod S number of particles always reside at the background of commensurate filling, the on-site interaction interfere the localization process in the presence of secondary lattice. We observe strong on-site repulsion forms dimer structure in the densities. We consider two specific cases: eight particles in seven lattice i.e, one extra particle

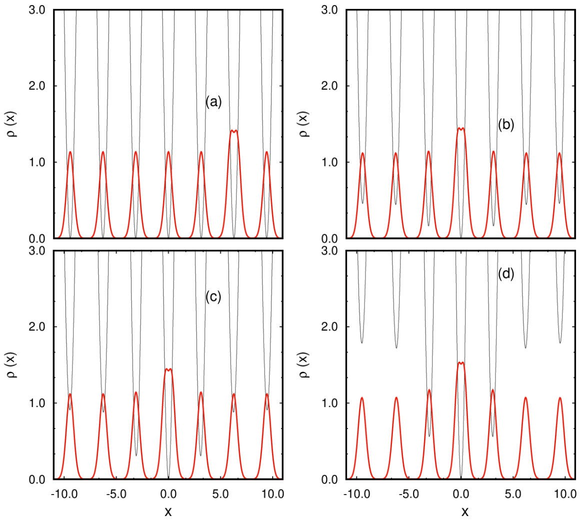

FIG. 6. The one-body density $\rho(x)$ for eight bosons in seven sites for interaction strength $\lambda = 10E_r$ and for various quasiperiodic parameter: $V_d = 0E_r$ [(a)], $V_d = 0.5E_r$ [(b)], $V_d = 1E_r$ [(c)], $V_d = 2E_r$ [(d)]. For each case, the gray curve presents the corresponding disordered lattice potential.

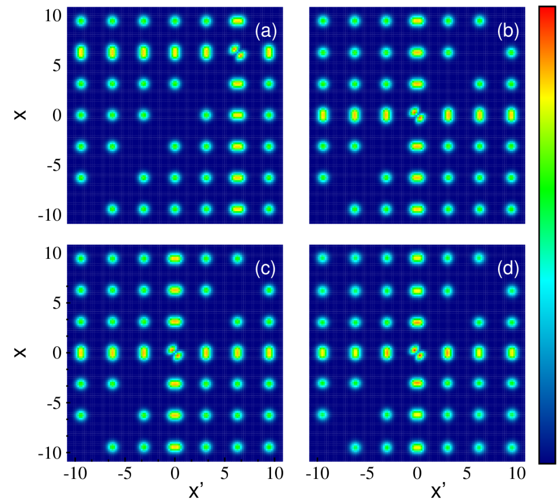

FIG. 7. Behavior of the reduced two-body density $\rho^{(2)}(x, x')$ for eight bosons in seven wells with interaction strength $\lambda = 10E_r$. The panels show the comparison between the periodic [(a) $V_d = 0E_r$] and quasiperiodic cases [(b) $V_d = 0.5E_r$, (c) $V_d = 1E_r$, (d) $V_d = 2E_r$].

added to the unit filling case and nine particles in seven lattice i.e., a pair of repulsive particles sits on a unit filling background. In the presence of disordered lattice; localization, delocalization and on-site interaction interplay in a complex way.

1. *One extra particle on localized background*

The top panel of Fig. 5 represents the ground state density in the clean lattice for eight particles distributed over seven lattice sites. For noninteracting case, the density is non uniform and centrally localized. For weak interaction, $\lambda = 0.5E_r$, the nonuniform occupation tends to become uniform (not shown here). For higher interaction, $\lambda = 3E_r$ (not shown here), we also observe a predominant occupation in a side well, signifying localization of the extra particle while the uniform Mott background exists. For much higher interaction, $\lambda = 10E_r$, the on-site repulsion is dominating. The onset of fermionization is mimicked by the formation of characteristic dip in the density distribution. In terms of fragmentation, the pair of interacting particles occupy two orbitals in the same well. To understand the scenario, one needs to go beyond Bose-Hubbard analysis when higher band contributions need to be taken into account. According to this, when seven particles occupy the lowest band forming an MI background of one particle localized in one well, the extra particle lies on the energetically lowest one-particle level of excited band [38]. Thus, the extra one delocalized particle does not allow a perfect insulator phase.

In Figs. 6(a)-(d), we present the one-body density in the fermionization limit $\lambda = 10E_r$ in presence of disorder, $V_d = 0E_r, 0.5E_r, 1E_r, 2E_r$ respectively. The pair of interacting bosons relocates the lattice site in the disordered lattice, however, the commensurate background of the insulating phase with seven particles localized in the seven lattice sites remains unchanged. It is also to mention that for weaker interaction, when on-site effect is not predominating, the introduced disorder easily competes with the weakly correlated Mott background surrounded by superfluid layer leading to localization in the central wells (not shown here).

In Fig. 7(a)-(d), we present the two-body density for periodic as well as for different disorder potentials in the fermionization limit. As stated before that completely depleted diagonal and the off-diagonal correlation is the hallmark of MI phase. In Fig. 7(a), in the periodic lattice [$V_d = 0E_r$], Mott dimerization happens in a corner lattice. The depleted diagonal with a dimer formation exhibits that while seven particles form the MI background, the extra particle sits on top of it. In quasiperiodic lattice $V_d = 0.5E_r$ (Fig. 7(b)) the dimer is settled in the central lattice when the depleted diagonal remains unchanged signifying the Mott background does not loose any correlation. For higher disorder strength $V_d = 1E_r$ (Fig. 7(c)) and $V_d = 2E_r$ (Fig. 7(d))the position of the dimer does not change anymore. We also do not find any loss of Mott correlation in the range of correlated disorder we probe.

2. *Two extra particles on localized background*

Next we consider the case when a repulsive pair of particles resides on a localized background, nine particles settle in seven lattice sites. The bottom panel of Fig. 5 presents the one-body density $\rho(x)$ in the primary lattice for various interaction strength. The solid red line represent the noninteracting case where nonuniform distribution is displayed. In the fermionization limit, $\lambda = 10E_r$, the many-body state is again a Mott dimerized state, but due to two extra particles, two dimers are formed in two sites. The characteristic dips signify that localized pairs are now fragmented.

The one- and two-body correlation in the fermionization limit is presented in Fig. 8. Some distinct features are expected as the two extra particles will now experience intra-pair repulsive force as well as repulsion due to the Mott background. For weaker interaction (not shown here) the off diagonal two-body correlation exists across the periodic lattice. Additional disorder leads to destroy the long-range correlation gradually. In the fermionization limit, $\lambda = 1 with 0E_r$, the one-body correlation displays seven bright lobes along the diagonal and complete extinction of off-diagonal correlation. However, the lobes are not of uniform coherence, they are brighter in the two corner lattice sites signifying the localization of two extra particles (Fig. 8(a)). In the two-body correlation function, the off-diagonal correlation is maintained and dimer structure with clear extinction of diagonal confirms the fragmented dimerization (Fig. 8(b)). For weaker interactions (not shown here), we have observed the dimers appear but without the correlation hole signifying that the pairing bosons are not fragmented. By "corelation hole" we mean $\rho^{(2)}(x, x') \to 0$, implying that the probability of finding two bosons in the same place is reduced. This resembles the behavior of hard-core bosons with infinitely strong contact interactions. In the fermionization limit the dimers are more correlated due to combined effect of strong intra-pair interaction as well as strong interaction with the Mott background. Now weak disorder ($V_d = 0.5E_r$) does not affect the background Mott correlation, only the dimer changes their location (Fig. 8(c)-(d)). However for stronger disorders ($V_d = 1E_r$ and $2E_r$), we observe reduction in Mott correlation as well as the dimers shift the lattice sites (Fig. 8(e)-(h)).

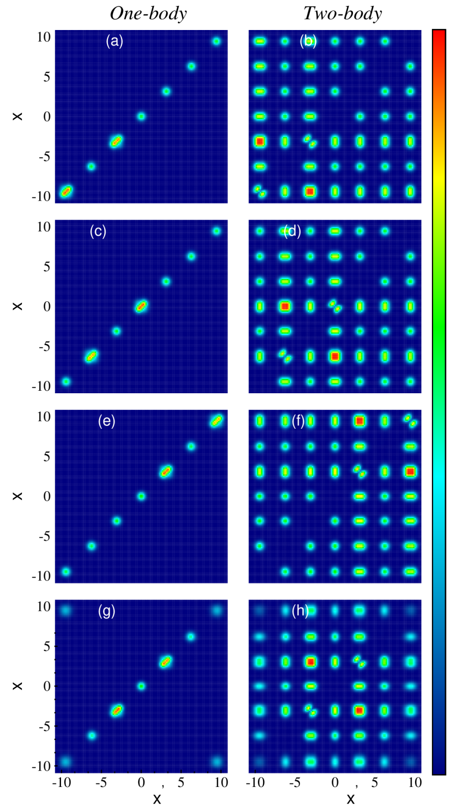

FIG. 8. The reduced one-body density $\rho^{(1)}(x, x')$ and two-body density $\rho^{(2)}(x, x')$ for nine bosons in seven wells with interaction strength $\lambda = 10E_r$. The panels show comparison between periodic case [$V_d = 0E_r$, panels (a)-(b)] and the quasiperiodic cases [panels (c)-(h)]; $V_d = 0.5E_r$ [(c)-(d)], $V_d = 1E_r$ [(e)-(f)], $V_d = 2E_r$ [(g)-(h)]

VI. CONCLUSION

We have demonstrated the effect of disorder in a few-boson systems in finite 1D lattice for different filling factors and varying strength of the repulsive interactions. Our study reveals a rich interplay between quasiperiodic disorder and filling factor. We have performed a numerically exact investigation and the interplay between interaction, disorder and incommensuration is presented by the measures of fragmentation, one- and two-body correlation. For the commensurate filling, we observe the expected physics: disorder introduced localization happens in noninteracting and very weakly interacting superfluid. Whereas, for strong repulsive interaction, the strongly correlated fragmented Mott localization remains robust, maintaining its structural integrity even under strong disorder strength.

However for incommensurate filling our study uncovers more intriguing interplay between disorder and interaction strength. It unravels some features not observed for commensurate filling. For the incommensurate filling in the primary lattice, the initial state is partially delocalized and incoherent depending on the number of particles and interaction strength. In particular, for filling factor less than one, the existing delocalization introduces imperfect localization in the primary lattice. In the strongly interacting limit, through fragmentation we establish that the many-body state is a fragmented superfluid. Introduced disorder tries to eliminate the superfluid layer and establish a insulating phase. The measure of order parameter establishes that disorder introduces a many-body state which is fully localized and S-fold fragmented. This highlights the fundamental role played by the secondary lattice to stabilize and create more coherent many-body state. We observe more interesting physics for filling factor grater than one, when the degree of localization of these extra particles is determined by the interaction strength. In the fermionization limit, Mott dimerization happens in the primary lattice- dimers with clear correlation hole is observed in the two-body correlation function. Disorder first pushes the dimer from one lattice to next lattice, without affecting the intra-pair correlation in the dimer, the background Mott correlation also remains unaffected. Stronger disorder is able to reduce Mott correlation. Our study explores some unconventional localization process in the strongly correlated systems.

From an experimental perspective, our predictions can be tested in the current ultracold atomic experiments. State-of-the-art techniques allow for the realization of quasiperiodic optical lattices with precisely tunable disorder strengths, the filling factor can also be tuned. Our study suggests clear experimental signatures, such as density redistribution patterns, one- and two-body correlations, which can be directly measured using quantum gas microscopy. The immediate extension of the present work is to investigate the long-range interacting many-body systems in the disordered lattice. Future works in this direction also include dynamically controlling the disorder and monitoring the dynamical evolution of the system in disordered lattice.

ACKNOWLEDGMENTS

BC acknowledges significant discussion of results with P. Molignini. BC and AG thank Fundação de Amparo à Pesquisa do Estado de São Paulo (FAPESP), grant nr. 2023/06550-4. AG also thanks the funding from Conselho Nacional de Desenvolvimento Científico e Tecnológico (CNPq), grant nr. 306219/2022-0.

Appendix A: The Multiconfigurational Time dependent Hartree method for bosons

The time-dependent many-body Schrödinger equation is given by

$$\hat{H}\Psi = i\hbar\frac{\partial\Psi}{\partial t} \tag{A1}$$

The many-body wave function is further decomposed as the linear combination of time dependent permanents

$$|\Psi(t)\rangle = \sum_{\bar{n}} C_{\bar{n}}(t)|\bar{n};t\rangle, \tag{A2}$$

The vector $|\vec{n};t\rangle = |n_1, ..., n_M;t\rangle; \sum_i n_i = N$. Thus the vector $\vec{n} = (n_1, n_2, \ldots, n_M)$ represents the occupation of each orbital, which ensures the preservation of the total number of particles. Distributing N bosons over M time dependent orbitals, the number of permanents become $\begin{pmatrix} N+M-1 \\ N \end{pmatrix}$. The permanents are constructed over M time-dependent single-particle wave functions, called orbitals, as

$$|\bar{n};t\rangle = \prod_{k=1}^{M}\left[\frac{(\hat{b}_k^\dagger(t))^{n_k}}{\sqrt{n_k!}}\right]|0\rangle \tag{A3}$$

Where $|0\rangle$ is the vacuum state and $\hat{b}_k^\dagger(t)$ denotes the time-dependent operator that creates one boson in the k-th working orbital $\psi_k(x)$, *i.e.*:

$$\hat{b}_k^\dagger(t) = \int \mathrm{d}x\, \psi_k^*(x;t)\hat{\Psi}^\dagger(x;t) \tag{A4}$$

$$\hat{\Psi}^\dagger(x;t) = \sum_{k=1}^{M}\hat{b}_k^\dagger(t)\psi_k(x;t). \tag{A5}$$

It is important to mention that the expansion coefficients $C_{\vec{n}}(t)$ and the orbitals that build up the configuration $|\vec{n};t\rangle$ are time-dependent and variationally optimized at every time step [52]. This requires the stationarity of the action with respect to variations of the time-dependent coefficients and orbitals. We employ the Dirac-Frenkel time-dependent variational [52], that leads to a set of coupled integro-differential equations in the variational parameters, the expansion coefficients $\{C_{\bar{n}}(t)\}$ and the working orbitals $\psi_i(x,t)$, which are then solved simultaneously. Note that the orbital and the coefficient $C_{\vec{n}}(t)$ are variationally optimal with respect to all parameters of the many-body Hamiltonian at any time [52–55]. Solving these differential equations with optimized methods in imaginary time allows us to compute the ground state while real time propagation leads to time evolution of a given initial state. As the permanents are time-dependent, a given degree of accuracy is achieved with shorter time compared to a time-independent basis. The time-adaptive basis allows the sampled Hilbert space to dynamically follow the motion under any quench process. Thus the time-dependent optimization of the orbitals and expansion coefficients ensure that the MCTDHB method can accurately describe the dynamics of strongly interacting bosons. Imaginary time propagation relaxes the system to its ground state.

MCTDHB has found extensive application in elucidating the statics and dynamics of various trap geometries and interaction strengths [56–62].

Appendix B: Convergence in the initial density

The accuracy of MCTDHB ansatz strictly depends on the choice of the number of orbitals M employed in the computation. In the limit of $M \to \infty$, the wave function becomes exact by construction and numerically it is achieved employing a finite number of orbitals for which the calculated observables exhibit convergence with respect to orbital numbers. In Fig. 9, we plot the density profile for different incommensurate filling factor with increasing orbital numbers. We specifically focus for the strongly interacting limit, convergence is established with

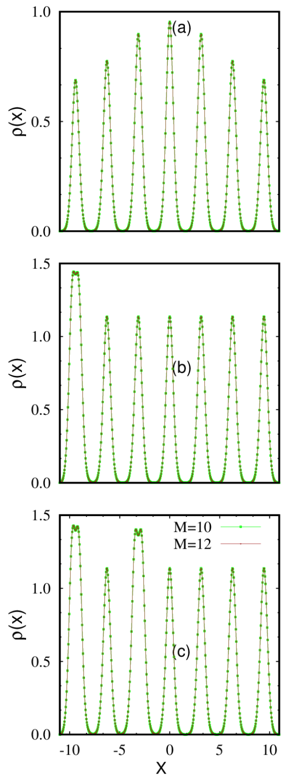

FIG. 9. One-body density $\rho(x)$ for different orbitals (M) for seven lattice sites in the primary lattice and for different incommensurate filling. (a) corresponds to five bosons with $\lambda = 5E_r$; (b) corresponds to eight bosons with $\lambda = 10E_r$ and (c) corresponds to nine bosons with $\lambda = 10E_r$

$M = 10$ and $M = 12$ orbitals. Fig. 9(a) corresponds to five bosons in seven lattice sites with $\lambda = 5E_r$; Fig. 9(b) corresponds to eight bosons in seven lattice sites with $\lambda = 10E_r$; Fig. 9(c) corresponds to nine bosons in seven lattice sites with $\lambda = 10E_r$. For all cases, density profiles with $M = 10$ and 12 are indistinguishable. Throughout our calculation we keep $M = 12$ orbitals irrespective of filling factors.

Appendix C: System parameters

The quasi periodic lattice is the superposition of two optical lattices; a primary lattice of depth V_p and wavelength λ_p and a secondary lattice of depth V_d and wavelength λ_d parameterized as

$$V(x) = V_p \sin^2(k_p x) + V_d \sin^2(k_d x) \tag{C1}$$

where k_i is the wave vector. We choose $\lambda_p \simeq 1032$ nm and $\lambda_d \simeq 862$ nm, which are compatible with real experimental realizations in ultracold atomic gases. These give vectors $k_p \simeq 6.088 \times 10^6$ m^{-1} and $k_d \simeq 7.289 \times 10^6$ m^{-1}. We set hard-wall boundaries to restrict the optical lattice to the center-most seven minima.

Quantity	MCTDH-X units
unit of length	$L = \lambda_p/3 = 344$ nm
unit of energy	$\bar{E} = \frac{\hbar^2}{2m\bar{L}^2} = E_r(\frac{3}{\pi})^2$
potential depth	$V = 10.0E \approx 9.128E_r$
on-site repulsion	$\lambda = 0.5E \approx 0.456E_r$

TABLE I. Units used in MCTDH-X simulations. $E_r = \frac{\hbar^2 k_p^2}{2m}$ is the recoil energy.

1. Lengths

In MCTDH-X simulations, we choose to set the unit of length $\bar{L} \equiv \frac{\lambda_p}{3} = 344$ nm, which makes the minima of the primary lattice appear at integer values in dimensionless units, while the maxima are located at half integer values. $x = 0$ is the center of the lattice which can host an odd number of lattice sites S. In our numerical simulation, we consider $S = 7$ sites and we run simulations with 512 grid points.

2. Energies

The unit of energy $\bar{E}$ is defined in terms of the recoil energy of the primary lattice, i.e. $E_r \equiv \frac{\hbar^2 k_p^2}{2m} \simeq 3.182 \times 10^{-26}$ J with $m \simeq 38.963$ Da, the mass of ^{39}K atoms. Thus we define the unit of energy as $\bar{E} \equiv \frac{\hbar^2}{2mL^2}$ $= E_r(\frac{3}{\pi})^2 = 2.904 \times 10^{-26}$ J. In typical experiments with quasi periodic optical lattice the depth of the primary lattice is varied in the around few tens of recoil energies and the depth of the secondary lattice is varied around few recoil energy. In our simulations, we probe similar regimes: V_p= $10E_r$ and $V_d \in [0E_r, 3E_r]$. The on-site interactions are kept fixed $\lambda = 0.5E_r$ for weakly interacting, $\lambda = 5E_r$ for strongly interacting limit and $\lambda = 10E_r$ for fermionization limit, these values can be achieved in the ultracold quantum simulators.

3. Time

The unit of time is defined from the unit of length as $\bar{t} \equiv \frac{2m\bar{L}^2}{\hbar} = \frac{2m{\lambda_p}^2}{\hbar} = 0.1307\ 10^{-4}$ s. $= 13.07\mu s$.

[1] M. P. A. Fisher, P. B. Weichman, G. Grinstein, and D. S. Fisher, Boson localization and the superfluid-insulator transition, Phys. Rev. B **40**, 546 (1989).

[2] M. Greiner, O. Mandel, T. Esslinger, T. W. Hänsch, and I. Bloch, Quantum phase transition from a superfluid to a mott insulator in a gas of ultracold atoms, Nature **415**, 39 (2002).

[3] M. Greiner, O. Mandel, T. W. Hansch, and I. Bloch, Collapse and revival of the matter wave field of a Bose–Einstein condensate, Nature **419**, 51 (2002).

[4] A. A. Burkov, Fractional quantum hall effect and featureless mott insulators, Phys. Rev.B **81**, 125111 (2010).

[5] T. Luibrand, L. Fratino, F. Tahouni-Bonab, A. Kronman, Y. Kalcheim, I. K. Schuller, M. Rozenberg, R. Kleiner, D. Koelle, and S. Guénon, Laser-induced quenching of metastability at the mott insulator to metal transition, Phys. Rev.B **110**, L081108 (2024).

[6] S. Sen, P. J. Wong, and A. K. Mitchell, The mott transition as a topological phase transition, Phys. Rev.B **102**, 081110(R) (2020).

[7] D. A. Abanin, E. Altman, I. Bloch, and M. Serbyn, Colloquium: Many-body localization, thermalization, and entanglement, Rev. Mod. Phys. **91**, 021001 (2019).

[8] V. Oganesyan and D. A. Huse, Localization of interacting fermions at high temperature, Phys. Rev.B **75**, 155111 (2020).

[9] T. Giamarchi and H. J. Schulz, Anderson localization and interactions in one-dimensional metals, Phys. Rev. B **37**, 325 (1988).

[10] J. E. Lye, L. Fallani, M. Modugno, D. S. Wiersma, C. Fort, and M. Inguscio, Bose-Einstein condensate in a random potential, Phys. Rev. Lett. **95**, 070401 (2005).

[11] H. Yao, A. Khoudli, L. Bresque, and L. Sanchez-Palencia, Critical behavior and fractality in shallow one-dimensional quasiperiodic potentials, Phys. Rev. Lett. **123**, 070405 (2019).

[12] M. Pasienski, D. McKay, M. White, and B. DeMarco, A disordered insulator in an optical lattice, Nature Phys. **6**, 677 (2010).

[13] H. Yao, T. Giamarchi, and L. Sanchez-Palencia, Lieb-Liniger bosons in a shallow quasiperiodic potential: Bose glass phase and fractal Mott lobes, Phys. Rev. Lett. **125**, 060401 (2020).

[14] H. Yao, L. Tanzi, L. Sanchez-Palencia, T. Giamarchi, G. Modugno, and C. D'Errico, Mott transition for a Lieb-Liniger gas in a shallow quasiperiodic potential: Delocalization induced by disorder, Phys. Rev. Lett. **133**, 123401 (2024).

[15] P. Lugan, D. Clément, P. Bouyer, A. Aspect, and L. Sanchez-Palencia, Anderson localization of Bogolyubov quasiparticles in interacting Bose-Einstein condensates, Phys. Rev. Lett. **99**, 180402 (2007).

[16] P. Lugan and L. Sanchez-Palencia, Localization of Bogoliubov quasiparticles in interacting Bose gases with correlated disorder, Phys. Rev. A **84**, 013612 (2011).

[17] J. Billy, V. Josse, Z. Zuo, A. Bernard, B. Hambrecht, P. Lugan, D. Clément, L. Sanchez-Palencia, P. Bouyer, and A. Aspect, Direct observation of Anderson localization of matter waves in a controlled disorder, Nature **453**, 891 (2008).

[18] L. Sanchez-Palencia, D. Clément, P. Lugan, P. Bouyer, G. V. Shlyapnikov, and A. Aspect, Anderson localization of expanding Bose-Einstein condensates in random potentials, Phys. Rev. Lett. **98**, 210401 (2007).

[19] P. Lugan, D. Clément, P. Bouyer, A. Aspect, M. Lewenstein, and L. Sanchez-Palencia, Ultracold Bose gases in 1d disorder: From Lifshits glass to Bose-Einstein condensate, Phys. Rev. Lett. **98**, 170403 (2007).

[20] L. Fallani, J. E. Lye, V. Guarrera, C. Fort, and M. Inguscio, Ultracold atoms in a disordered crystal of light: Towards a Bose glass, Phys. Rev. Lett. **98**, 130404 (2007).

[21] Z. Zhu, H. Yao, and L. Sanchez-Palencia, Thermodynamic phase diagram of two-dimensional bosons in a quasicrystal potential, Phys. Rev.Lett. **130**, 220402 (2023).

[22] G. Roux, T. Barthel, I. P. McCulloch, C. Kollath, U. Schollwöck, and T. Giamarchi, Quasiperiodic bose-hubbard model and localization in one-dimensional cold atomic gases, Phys. Rev. A **78**, 023628 (2008).

[23] R. Gautier, H. Yao, and L. Sanchez-Palencia, Strongly interacting bosons in a two-dimensional quasicrystal lattice, Phys. Rev. Lett. **126**, 110401 (2021).

[24] G. Roati, C. D'Errico, L. Fallani, M. Fattori, C. Fort, M. Zaccanti, G. Modugno, M. Modugno, and M. Inguscio, Anderson localization of a non-interacting Bose–Einstein condensate, Nature **453**, 895 (2008).

[25] L. Sanchez-Palencia and M. Lewenstein, Disordered quantum gases under control, Nat. Phys. **6**, 87 (2010).

[26] G. Modugno, Anderson localization in Bose–Einstein condensates, Rep. Prog. Phys. **73**, 102401 (2010).

[27] C. D'Errico and M. G. Tarallo, One-dimensional disordered bosonic systems, Atoms **9**, 112 (2021).

[28] C. D'Errico, E. Lucioni, L. Tanzi, L. Gori, G. Roux, I. P. McCulloch, T. Giamarchi, M. Inguscio, and G. Modugno, Observation of a disordered bosonic insulator from weak to strong interactions, Phys. Rev. Lett. **113**, 095301 (2014).

[29] B. Chakrabarti, A. Gammal, and L. Salasnich, Strongly interacting bosons in a one-dimensional disordered lattice: Phase coherence of distorted mott phases, Phys. Rev. B **110**, 184202 (2024).

[30] M. Reetz-Lamour, T. Amthor, J. Deiglmayr, and M. Weidem¨uller, Rabi oscillations and excitation trap- ping in the coherent excitation of a mesoscopic frozen rydberg gas, Phys. Rev. Lett. **100**, 253001 (2008).

[31] M. Reetz-Lamour, J. Deiglmayr, T. Amthor, and M. Weidem¨uller, Rabi oscillations between ground and rydberg states and van der waals blockade in a meso- scopic frozen rydberg gas, New Jour. Phys. **10**, 045026 (2008).

[32] J.-P. Brantut, J. Meineke, D. Stadler, S. Krinner, and T. Esslinger, Conduction of ultracold fermions through a mesoscopic channel,, Science **337**, 1069 (2012).

[33] J. Zeiher, J. Wolf, J. A. Isaacs, J. Kohler, and D. M. Stamper-Kurn, Tracking evaporative cooling of a mesoscopic atomic quantum gas in real time, Phys. Rev. X **11**, 041017 (2021).

[34] Y. Wang, S. Shevate, T. M. Wintermantel, M. Morgado, G. Lochead, and S. Whitlock, Preparation of hundreds of microscopic atomic ensembles in optical tweezer ar- rays, npj Quantum Information **6**, 54 (2020).

[35] L. Pizzino, H. Yao, and T. Giamarchi, Finite size analysis for interacting bosons at the one-two dimensional crossover, Phys. Rev. Research **7**, 013021 (2025).

[36] I. Bloch, J. Dalibard, and W. Zwerger, Many-body physics with ultracold gases, Rev. Mod. Phys. **80**, 885 (2008).

[37] A. Polkovnikov, K. Sengupta, A. Silva, and M. Vengalattore, Colloquium: Nonequilibrium dynamics of closed interacting quantum systems, Rev. Mod. Phys. **83**, 863 (2011).

[38] I. Brouzos, S. Zöllner, and P. Schmelcher, Correlation versus commensurability effects for finite bosonic systems

in one-dimensional lattices, Phys. Rev. A **81**, 053613 (2010).

[39] M. H. Beck, A. Jäckle, G. A. Worth, and H.-D. Meyer, The multiconfiguration time-dependent Hartree (MCTDH) method: a highly efficient algorithm for propagating wavepackets, Phys. Rep. **324**, 1 (2000).

[40] J.-G. Baak and U. R. Fischer, Self-consistent many-body metrology, Phys. Rev. Lett. **132**, 240803 (2024).

[41] S. K. Adhikari and L. Salasnich, Localization of a Bose-Einstein condensate in a bichromatic optical lattice, Phys. Rev. A **80**, 023606 (2009).

[42] A. I. Streltsov, O. E. Alon, and L. S. Cederbaum, General variational many-body theory with complete self-consistency for trapped bosonic systems, Phys. Rev. A **73**, 063626 (2006).

[43] A. I. Streltsov, O. E. Alon, and L. S. Cederbaum, Role of excited states in the splitting of a trapped interacting Bose-Einstein condensate by a time-dependent barrier, Phys. Rev. Lett. **99**, 030402 (2007).

[44] O. E. Alon, A. I. Streltsov, and L. S. Cederbaum, Unified view on multiconfigurational time propagation for systems consisting of identical particles, J. Chem. Phys. **127**, 154103 (2007).

[45] O. E. Alon, A. I. Streltsov, and L. S. Cederbaum, Multiconfigurational time-dependent Hartree method for bosons: Many-body dynamics of bosonic systems, Phys. Rev. A **77**, 033613 (2008).

[46] A. U. J. Lode, Multiconfigurational time-dependent Hartree method for bosons with internal degrees of freedom: Theory and composite fragmentation of multi-component Bose-Einstein condensates, Phys. Rev. A **93**, 063601 (2016).

[47] E. Fasshauer and A. U. J. Lode, Multiconfigurational time-dependent Hartree method for fermions: Implementation, exactness, and few-fermion tunneling to open space, Phys. Rev. A **93**, 033635 (2016).

[48] R. Lin, P. Molignini, L. Papariello, M. C. Tsatsos, C. Lévêque, S. E. Weiner, E. Fasshauer, and R. Chitra, MCTDH-X: The multiconfigurational time-dependent Hartree method for indistinguishable particles software, Quantum Sci. Technol. **5**, 024004 (2020).

[49] A. U. J. Lode, M. C. Tsatsos, E. Fasshauer, S. E. Weiner, R. Lin, L. Papariello, P. Molignini, C. Lévêque, M. Büttner, J. Xiang, S. Dutta, and Y. Bilinskaya, MCTDH-X: The multiconfigurational time-dependent Hartree method for indistinguishable particles software (2024).

[50] B. Chatterjee and A. U. J. Lode, Order parameter and detection for a finite ensemble of crystallized one-dimensional dipolar bosons in optical lattices, Phys. Rev. A **98**, 053624 (2018).

[51] O. Penrose and L. Onsager, Bose-Einstein condensation and liquid helium, Phys. Rev. **104**, 576 (1956).

[52] P. Kramer and M. Saraceno, *Geometry of the Time-Dependent Variational Principle in Quantum Mechanics*, Lecture Notes in Physics, Vol. 140 (Springer, 1981).

[53] S. Kvaal, Variational formulations of the coupled-cluster method in quantum chemistry, Mol. Phys. **111**, 1100 (2013).

[54] A. McLachlan, A variational solution of the time-dependent Schrödinger equation, Mol. Phys. **8**, 39 (1964).

[55] L. Cao, V. Bolsinger, S. I. Mistakidis, G. M. Koutentakis, S. Krönke, J. M. Schurer, and P. Schmelcher, A unified ab initio approach to the correlated quantum dynamics of ultracold fermionic and bosonic mixtures, J. Chem. Phys. **147**, 044106 (2017).

[56] R. Roy, A. Gammal, M. C. Tsatsos, B. Chatterjee, B. Chakrabarti, and A. U. J. Lode, Phases, many-body entropy measures, and coherence of interacting bosons in optical lattices, Phys. Rev. A **97**, 043625 (2018).

[57] S. Bera, R. Roy, A. Gammal, B. Chakrabarti, and B. Chatterjee, Probing relaxation dynamics of a few strongly correlated bosons in a 1d triple well optical lattice, J. Phys. B: Atom., Mol. Opt. **52**, 215303 (2019).

[58] R. Roy, B. Chakrabarti, N. D. Chavda, and M. L. Lekala, Information theoretic measures for interacting bosons in optical lattice, Phys. Rev. E **107**, 024119 (2023).

[59] R. Roy, B. Chakrabarti, and A. Gammal, Out of equilibrium many-body expansion dynamics of strongly interacting bosons, SciPost Phys. Core **6**, 073 (2023).

[60] P. Molignini and B. Chakrabarti, Unbounded entropy production and violent fragmentation for repulsive-to-attractive interaction quench in long-range interacting systems, New J. Phys. **26**, 103030 (2024).

[61] P. Molignini and B. Chakrabarti, Interaction quench of dipolar bosons in a one-dimensional optical lattice, PHYSICAL REVIEW RESEARCH **7**, 013257 (2025).

[62] P. Molignini and B. Chakrabarti, Stability of dipolar bosons in a quasiperiodic potential, PHYSICAL REVIEW RESEARCH 7, 023237 (2025) **7**, 023237 (2025).